Takenori Inomata, Nobuyuki, Ebihara, Toshinari Funaki, Akira Matsuda, Yasuo Watanabe, Liang Ning, Zhuo Xu, Akira Murakami, and Eri Arikawa-Hirasawa,	Perlecan-Deficient Mutation Impairs Corneal Epithelial Structure	IOVS	Vol.53, No. 3	1277-1284	2012
Masuda A, Andersen HS, Doktor TK, Okamoto T, Ito M, Andresen BS, Ohno K.	CUGBP1 and MBNL1 preferentially bind to 3' UTRs and facilitate mRNA decay	*Sci Rep*	2	209	2012
Ito M, Suzuki Y, Okada T, Fukudome T, Yoshimura T, Masuda A, Takeda S, Krejci E, Ohno K.	Protein-anchoring strategy for delivering acetylcholinesterase to the neuromuscular junction	*Mol Ther*	20	1384-1392	2012
Ishigaki S, Masuda A, Fujioka Y, Iguchi Y, Katsuno M, Shibata A, Urano F, Sobue G, Ohno K.	Position-dependent fus-rna interactions regulate alternative splicing events and transcriptions	*Sci Rep*	2	529	2012
Sugie K, Hayashi YK, Goto K, Nishino I, Ueno S.	Unusual presentation: Unilateral arm and contralateral leg amyotrophy in FSHD.	Neurology	79(5)	e46	2012
Sugie K, Tonomura Y, Ueno S.	Characterization of dermatomyositis with coexistence of anti-Jo-1 and anti-SRP antibodies.	Intern Med	51(7)	799-802	2012

杉江和馬.	ライソゾーム病：ダノン病. 先天代謝異常症候群 一病因・病態研究、診断・治療の進歩ー.	日本臨床	20	588-592	2012
Momma K, Noguchi S, Malicdan MC, Hayashi YK, Minami N, Kamakura K, Nonaka I, Nishino I	Rimmed vacuoles in Becker muscular dystrophy have similar features with inclusion myopathies.	PLoS One.	7(12)	e52002	2012
Komagamine T, Kawai M, Kokubun N, Miyatake S, Ogata K, Hayashi YK, Nishino I, Hirata K	Selective muscle involvement in a family affected by a second LIM domain mutation of fhl1: An imaging study using computed tomography.	J Neurol Sci.	318(2012)	163-167	2012
Mori-Yoshimura M, Monma K, Suzuki N, Aoki M, Kumamoto T, Tanaka K, Tomimitsu H, Nakano S, Sonoo M, Shimizu J, Sugie K, Nakamura H, Oya Y, Hayashi YK, Malicdan MC, Noguchi S, Murata M, Nishino I	Heterozygous UDP-GlcNAc 2-epimerase and N-acetylmannosamine kinase domain mutations in the GNE gene result in a less severe GNE myopathy phenotype compared to homozygous N-acetylmannosamine kinase domain mutations.	J Neurol Sci.	318(2012):	100-105	2012

Nakamura M, Kaneko S, Ito H, Jiang S, Fujita K, Wate R, Nakano S, Fujisawa JI, Kusaka H.	Activation of Transforming Growth Factor-ß/Smad Signaling Reduces Aggregate Formation of Mislocalized TAR DNA-Binding Protein-43.	Neuro-degenerative diseases	:Jul 10. [Epub ahead of print]		2012
Nakamura S, Kaneko S, Shinde A, Morita JI, Fujita K, Nakano S, Kusaka H.	Prednisolone-sparing effect of cyclosporin A therapy for very elderly patients with myasthenia gravis.	Neuromuscular disorders : NMD	:Dec 10. [Epub ahead of print]		2012
Nakamura M, Kaneko S, Wate R, Asayama S, Nakamura Y, Fujita K, Ito H, Kusaka H.	Regionally different immunoreactivity for Smurf2 and pSmad2/3 in TDP-43-positive inclusions of amyotrophic lateral sclerosis.	Neuropathology and applied neurobiology	:Mar 21. [Epub ahead of print]		2012
Yamashita S, Mori A, Sakaguchi H, et al.	Sporadic juvenile amyotrophic lateral sclerosis caused by mutant FUS/TLS: possible association of mental retardation with this mutation.	J Neurol.	259(6)	1039-44	2012
Yamashita S, Sakaguchi H, Mori A, et al.	Significant CMAP decrement by repetitive nerve stimulation is more frequent in median than ulnar nerves of patients with amyotrophic lateral sclerosis.	Muscle Nerve	45(3)	426-8	2012

小牧宏文	小児の診療手技 100 筋生検	小児科診療	75	276-278	2012
小牧宏文	症候・疾患と検査・診断　神経筋疾患の診断	小児神経学の進歩	41	69-77	2012
石山昭彦, 小牧宏文	小児慢性疾患の生活指導－最新の知見から－　10.神経・筋疾患 2) 先天性ミオパチー	小児科臨床	65 巻 4 号	839-846	2012
石山昭彦, 藤義朗	先天性筋ジストロフィー	小児内科	44 巻増刊号	794-795	2012
佐々木良元、高橋正紀、穀内洋介、平山正昭、衣斐　達、冨本秀和、望月秀樹、佐橋　功	骨格筋型塩化物イオンチャネル遺伝子（CLCN1）の複合ヘテロ接合体変異で重症化した Thomsen 病	臨床神経学	印刷中		
Yoshinaga H, Sakoda S, Good J M, Takahashi M P, Kubota T, Arikawa-Hirasawa E, Nakata T, Ohno K, Kitamura T, Kobayashi K, Ohtsuka Y.	A novel mutation in *SCN4A* causes severe myotonia and school-age-onset paralytic episodes	*J Neurol Sci*	315	15-19	2012
Matsuura T, Minami N, Arahata H, Ohno K, Abe K, Hayashi YK, Nishino I.	Myotonic dystrophy type 2 is rare in the Japanese population	*J Hum Genet*	57	219-220	2012

Yamashita Y*, Matsuura T*, Shinmi J, Amakusa Y, Masuda A, Ito M, Kinoshita M, Furuya H, Abe K, Ibi T, Sahashi K, Ohno K.	Four parameters increase the sensitivity and specificity of the exon array analysis and disclose twenty-five novel aberrantly spliced exons in myotonic dystrophy	*J Hum Genet*	57	368-374	2012
Yamamoto R, Matsushita M, Kitoh H, Masuda A, Ito M, Katagiri T, Kawai T, Ishiguro N, Ohno K.	Clinically applicable antianginal agents suppress osteoblastic transformation of myogenic cells and heterotopic ossifications in mice	*J Bone Miner Metab*	31	26-33	2012
Ohe K, Masuda A, Ohno K.	Intronic and exonic nucleotide variations that affect rna splicing in humans	*Introduction to Sequence and Genome Analysis.* iConcept Press, Hong Kong		in press	2012
Mori-Yoshimura M, Monma K,Suzuki N, Aoki M, Kumamoto T, Tanaka K, Tomimitsu H, Nakano S, Sonoo M, Shimizu J,**Sugie K**, Nakamura H, Oya Y, Hayashi YK, Malicdan MC, Noguchi S, Murata M, Nishino I.	Heterozygous UDP-GlcNAc 2-epimerase and N-acetylmannosamine kinase domain mutations in the GNE gene result in a less severe GNE myopathy phenotype compared to homozygous N-acetylmannosamine kinase domain mutations.	J Neurol Sci	318(1-2)	100-105	2012

Sawa N, Kataoka H, **Sugie K**, Kawahara M, Horikawa H, Kusunoki S, Ueno S.	Clinical analysis and outcomes of amyotrophic lateral sclerosis with demyelinating polyneuropathy.	Amyotroph Lateral Scler	13(1)	125-31	2012
杉江和馬.	顔面肩甲上腕型筋ジストロフィーの骨格筋障害の分布.	難病と在宅ケア	17(10)	53-55	2012

Ⅴ．研究成果に関する刊行

ORIGINAL ARTICLE

Exome sequencing identifies a novel *TTN* mutation in a family with hereditary myopathy with early respiratory failure

Rumiko Izumi[1,2], Tetsuya Niihori[1], Yoko Aoki[1], Naoki Suzuki[2], Masaaki Kato[2], Hitoshi Warita[2],
Toshiaki Takahashi[3], Maki Tateyama[2], Takeshi Nagashima[4], Ryo Funayama[4], Koji Abe[5], Keiko Nakayama[4],
Masashi Aoki[2] and Yoichi Matsubara[1]

Myofibrillar myopathy (MFM) is a group of chronic muscular disorders that show the focal dissolution of myofibrils and accumulation of degradation products. The major genetic basis of MFMs is unknown. In 1993, our group reported a Japanese family with dominantly inherited cytoplasmic body myopathy, which is now included in MFM, characterized by late-onset chronic progressive distal muscle weakness and early respiratory failure. In this study, we performed linkage analysis and exome sequencing on these patients and identified a novel c.90263G>T mutation in the *TTN* gene (NM_001256850). During the course of our study, another groups reported three mutations in *TTN* in patients with hereditary myopathy with early respiratory failure (HMERF, MIM #603689), which is characterized by overlapping pathologic findings with MFMs. Our patients were clinically compatible with HMERF. The mutation identified in this study and the three mutations in patients with HMERF were located on the A-band domain of titin, suggesting a strong relationship between mutations in the A-band domain of titin and HMERF. Mutation screening of *TTN* has been rarely carried out because of its huge size, consisting of 363 exons. It is possible that focused analysis of *TTN* may detect more mutations in patients with MFMs, especially in those with early respiratory failure.
Journal of Human Genetics advance online publication, 28 February 2013; doi:10.1038/jhg.2013.9

INTRODUCTION

Myofibrillar myopathies (MFMs) were proposed in 1996 as a group of chronic muscular disorders characterized by common morphologic features observed on muscle histology, which showed the focal dissolution of myofibrils followed by the accumulation of products of the degradative process.[1] The clinical phenotype of MFM is characterized by slowly progressive muscle weakness that can involve proximal or distal muscles, with onset in adulthood in most cases. However, other phenotypes are highly variable. Although 20% of patients with MFMs have been revealed to have mutations in *DES*, *CRYAB*, *MYOT*, *LDB (ZASP)*, *FLNC* or *BAG3*, the major genetic basis of MFMs remains to be elucidated.

Respiratory weakness is one of the symptoms of MFMs. The early or initial presentation of respiratory failure is not a common manifestation of MFMs as a whole, and there are limited reports regarding a fraction of patients with *DES*,[2] *MYOT*[3] or *CRYAB*[4] mutation. In 1993,

our group reported a Japanese family with dominantly inherited cytoplasmic body (CB) myopathy,[5] which is now included in MFM. Currently, this family includes 20 patients in five successive generations who show almost homogeneous clinical features characterized by chronic progressive distal muscle weakness and early respiratory failure. However, the underlying genetic etiology in this family was unknown. The aim of this study was to determine the genetic cause in this family. To identify the responsible genetic mutation, we performed linkage analysis and whole-exome sequencing.

MATERIALS AND METHODS

This study was approved by the Ethics Committee of the Tohoku University School of Medicine, and all individuals gave their informed consent before their inclusion in the study.

[1]Department of Medical Genetics, Tohoku University School of Medicine, Sendai, Japan; [2]Department of Neurology, Tohoku University School of Medicine, Sendai, Japan; [3]Department of Neurology and Division of Clinical Research, National Hospital Organization Nishitaga National Hospital, Sendai, Japan; [4]Division of Cell Proliferation, United Centers for Advanced Research and Translational Medicine, Tohoku University Graduate School of Medicine, Sendai, Japan and [5]Department of Neurology, Okayama University Medical School, Okayama, Japan
Correspondence: Dr Y Aoki, Department of Medical Genetics, Tohoku University School of Medicine, 1-1 Seiryo-machi, Aoba-ku, Sendai 980-8574, Japan.
E-mail: aokiy@med.tohoku.ac.jp
or Professor M Aoki, Department of Neurology, Tohoku University School of Medicine, 1-1 Seiryo-machi, Aoba-ku, Sendai 980-8574, Japan.
E-mail: aokim@med.tohoku.ac.jp
Received 23 October 2012; revised 9 January 2013; accepted 10 January 2013

Clinical information on the family

This family includes 20 patients (13 males and 7 females) in five successive generations (Figure 1). The family is of Japanese ancestry, and no consanguineous or international mating was found. Of all patients, seven underwent a muscle biopsy, and two were autopsied. All of the histological findings were compatible with MFM (see clinical data).

The age of onset ranged from 27–45 years. The most common presenting symptom was foot drop. At the initial evaluations, muscle weakness was primarily distributed in the ankle dorsiflexors and finger extensors. The patients were generally built and showed no other extramuscular abnormalities. In addition to this chronic progressive distal muscle weakness, respiratory distress occurred between 0 and 7 years from the initial onset (average 3.8 years) in seven patients (IV-9, V-2, A, B, E, H, and J) with adequate clinical information. Two patients who had not had any respiratory care died of respiratory failure approximately a decade from the initial onset. The other patients have been alive for more than 10 years (maximum 18 years) but require nocturnal non-invasive positive pressure ventilation. They were 37–58 years of age as of 2012 and able to walk independently with or without a simple walking aid. Although the time at which patients recognized dysphagia or dysarthria varied between 1 to more than 10 years from the initial onset, decreased bulbar functions had been noted at the initial evaluation in most cases. Cardiac function was normally maintained in all patients of the family.

Clinical data

The level of serum creatine kinase was normal or mildly elevated. Electromyography of affected muscles showed a chronic myogenic pattern, and the nerve conduction study did not suggest any neuropathic involvement. Muscle imaging showed focal atrophy in the tibialis anterior, tibialis posterior, extensor hallucis and digitorum longus, peroneal and semitendinosus muscle on initial assessment (Figure 2A), and atrophy became clear in cervical muscles, shoulder girdles, intercostals and proximal limb muscles in the following several years. Upon muscle biopsy, the most common finding was numerous cytoplasmic bodies (CBs), which were found on 7.3% of myofibers in the tibialis anterior of individual E (Figure 2B (a–c)) and 50–80% of intercostals in other cases.[5]

Other nonspecific findings were increased variability in the size of myofibers, central nuclei and rimmed vacuoles observed on a few fibers. No strong immunoreaction of desmin was seen in the CBs (Figure 2B (d, e)). An electron microscope examination showed that the regular sarcoplasmic pattern was replaced by abnormal fine filamentous structures, which seemed to attach to the Z-band. CBs were also found in almost all skeletal muscles and some smooth muscles in autopsied cases.[5] Cardiac myofibers also contained numerous CBs in one of the autopsied cases (V-2),[5] although the patient did not present any cardiac complication. The sequence analysis of the coding regions and flanking introns of *DES* and *MYOT* showed no pathogenic mutation in individual E. An array comparative genomic hybridization performed with the Agilent SurePrint G3 Human CGH 1M microarray format in individual A did not reveal any aberrations of genomic copy number.

Linkage analysis

DNA was extracted by standard methods. Linkage analysis was performed on nine family members (A–I in Figure 1; four of them were affected, and the others were unaffected) through genotyping using an Illumina Human Omni 2.5 BeadChip (Illumina, San Diego, CA, USA). We chose single-nucleotide polymorphisms (SNPs) that satisfied all of the following criteria: (1) autosomal SNPs whose allele frequencies were available from the HapMap project (http://hapmap.ncbi.nlm.nih.gov/), (2) SNPs that were not monomorphic among members and (3) SNPs that were not in strong linkage disequilibrium with neighboring SNPs (r2 values <0.9). Then, we selected the first five SNPs from each position of integer genetic distance from SNPs that met the above criteria for the initial analysis. The details were as follows; we chose a SNP closest to 0 cM and the neighboring four SNPs. If the genetic distance of a SNP was the same as that of the next SNP, we considered the genomic position to determine their order. We repeated this process at 1 cM, 2 cM and so on.

We performed a multipoint linkage analysis of the data set (17 613 SNPs) using MERLIN[6] 1.1.2 under the autosomal dominant mode with the following parameters: 0.0001 for disease allele frequency, 1.00 for individuals heterozygous and homozygous for the disease allele and 0.00 for individuals
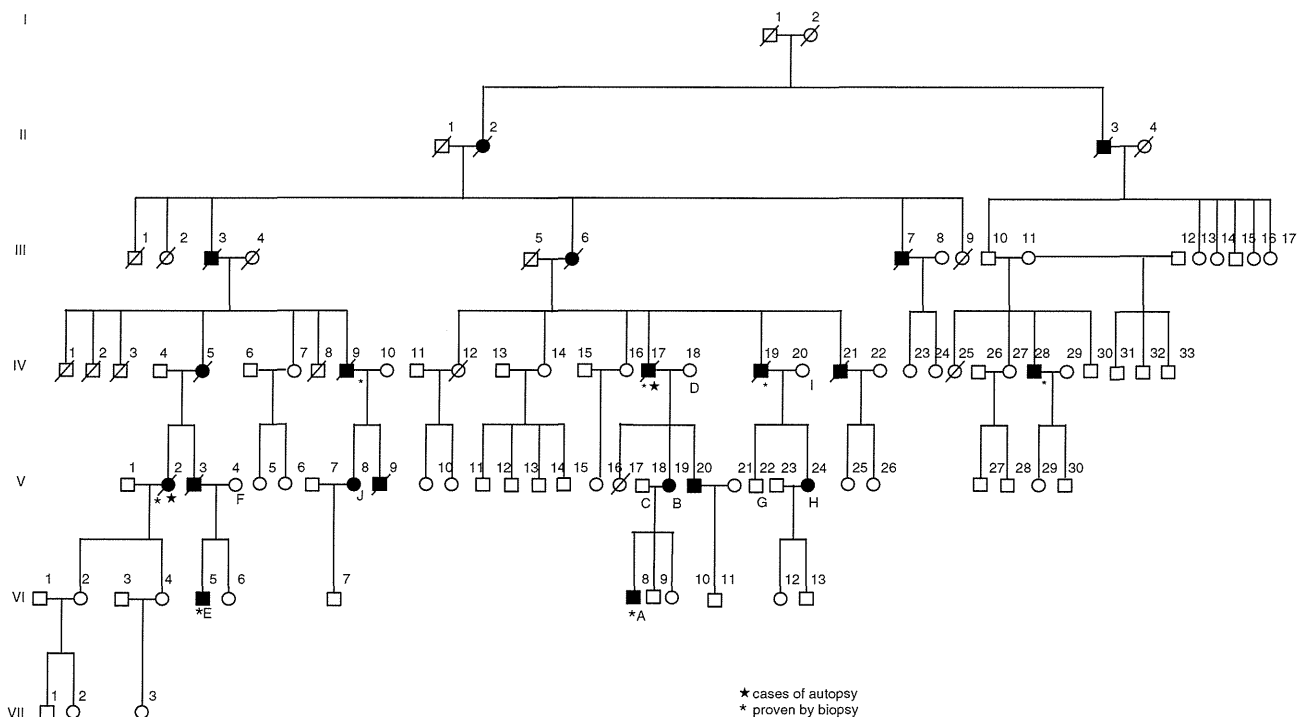

Figure 1 Family pedigree. Filled-in symbols indicate individuals with MFM. Empty symbols indicate unaffected individuals. A star and asterisk indicate autopsy-proven and muscle biopsy-proven cases, respectively. (A–J) indicates individuals whose DNA was used for this study.
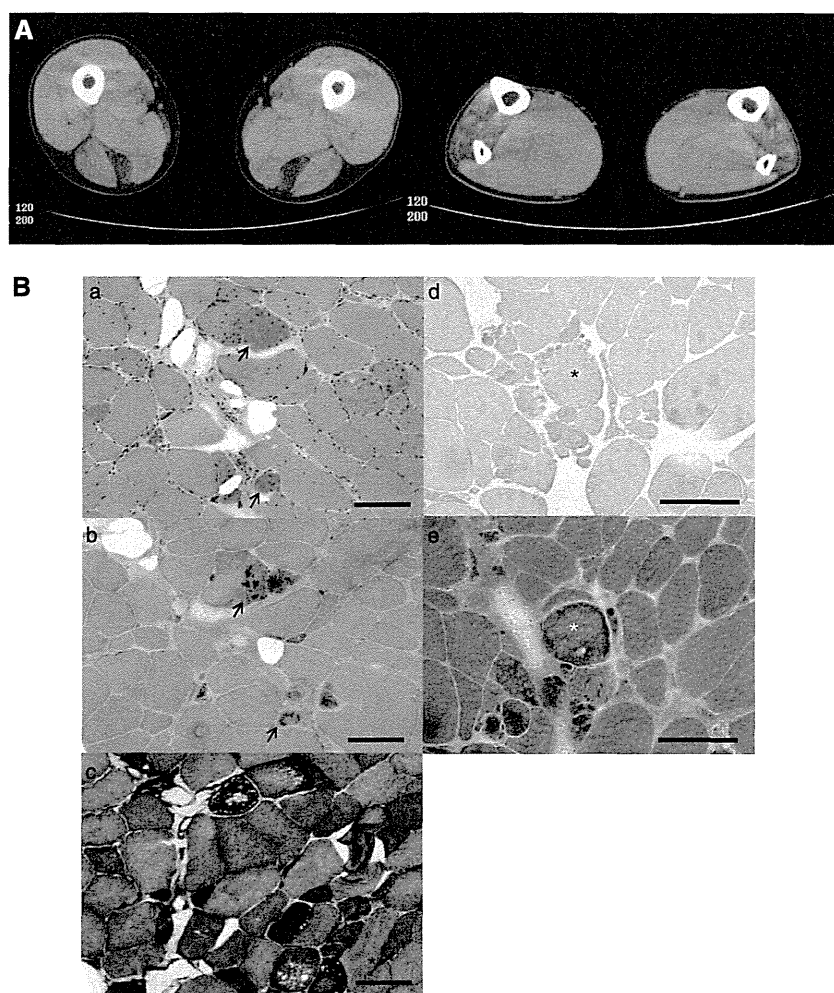
Figure 2 Family clinical data. (A) Muscle computed tomography of affected lower extremity. The imaging in the initial assessment of individual A showed symmetrical atrophy and fatty replacement of the semitendinosus in the proximal lower extremities (left) and the tibialis anterior, tibialis posterior, extensor hallucis and digitorum longus, and peroneal muscle in the distal (right) lower extremities. (B) Pathology of muscle biopsy. Hematoxylin-eosin (a), Gomori-trichrome (b) and NADH (nicotinamide adenine dinucleotide)-tetrazolium reductase (c) staining of the muscle biopsy sample from the tibialis anterior of individual E are shown. CBs are indicated by arrows. CBs were round or oval, 5–10 μm in diameter and predominantly located in the periphery of type 1 fibers, which stained eosinophilic with hematoxylin-eosin and blue–purple with Gomori-trichrome. NADH-tetrazolium reductase staining showed disorganization of the myofibrillar network. Immunostaining for desmin (d) and Gomori-trichrome staining (e) are serial sections of the muscle biopsy from individual E. Stars indicate corresponding fibers. No strong immunoreaction of desmin was seen in the CBs. Scale bars = 100 μm

homozygous for the alternative allele. After this first analysis, a second analysis was performed with all SNPs fulfilling the above criteria around the peaks identified in the first analysis.

Exome sequencing

Exome sequencing was performed on seven family members in three generations (A–E, H and I in Figure 1), four of whom were affected. Exon capture was performed with the SureSelect Human All Exon kit v2 (individuals E, H and I) or v4 (A–D) (Agilent Technologies, Santa Clara, CA, USA). Exon libraries were sequenced with the Illumina Hiseq 2000 platform according to the manufacturer's instructions (Illumina). Paired 101-base pair reads were aligned to the reference human genome (UCSChg19) using the Burrows-Wheeler Alignment tool.[7] Likely PCR duplicates were removed with the Picard program (http://picard.sourceforge.net/). Single-nucleotide variants and indels were identified using the Genome Analysis Tool Kit (GATK) v1.5 software.[8] SNVs and indels were annotated against the RefSeq database and dbSNP135 with the ANNOVAR program.[9] We used the PolyPhen2 polymorphism phenotyping software tool[10] to predict the functional effects of mutations.

Sanger sequencing

To confirm that mutations identified by exome sequencing segregated with the disease, we performed direct sequencing. PCR was performed with the primers shown in Supplementary Table 1. PCR products were purified with a MultiScreen PCR plate (Millipore, Billerica, MA, USA) and sequenced using BigDye terminator v1.1 and a 3500xL genetic analyzer (Applied Biosystems, Carlsbad, CA, USA).

RESULTS

Linkage analysis

The first linkage analysis identified five regions across autosomes with a logarithm of odds (LOD) score greater than 2 (Figure 3). Of the five regions, two were on chromosome 2 (from 167 cM to 168 cM, with a maximum LOD score of 2.46 and from 182 cM to 185 cM, with a maximum LOD score of 2.71), the other two were on chromosome 8 (from 27 cM to 34 cM, with a maximum LOD score of 2.71 and at 61 cM, with a maximum LOD score of 2.03), and one was on
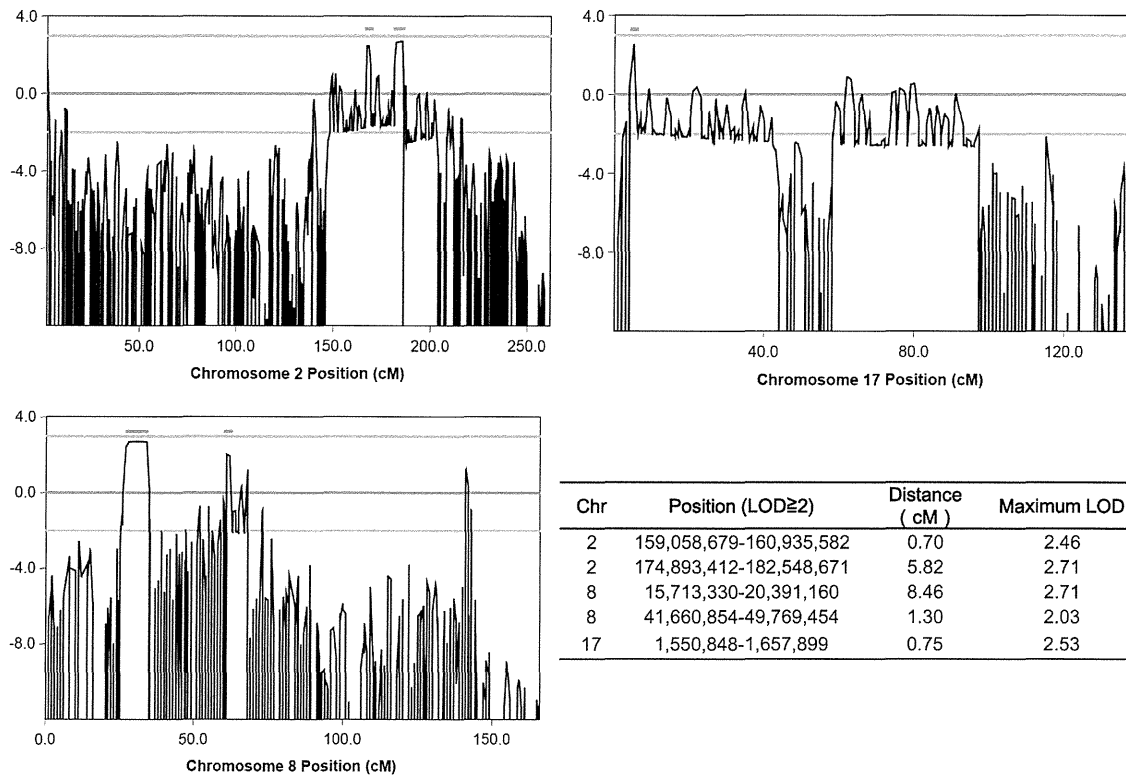
Chr	Position (LOD≧2)	Distance (cM)	Maximum LOD
2	159,058,679-160,935,582	0.70	2.46
2	174,893,412-182,548,671	5.82	2.71
8	15,713,330-20,391,160	8.46	2.71
8	41,660,854-49,769,454	1.30	2.03
17	1,550,848-1,657,899	0.75	2.53

Figure 3 Linkage analysis. Linkage analysis was performed on nine family members (four of them were affected, the others were unaffected) using an Illumina Human Omni 2.5 BeadChip. Five regions with an LOD score greater than 2 (indicated by bar) were identified. A full color version of this figure is available at the *Journal of Human Genetics* journal online.

Table 1 Summary of detected variants by exome sequencing

Individual Morbidity	A Affected	B Affected	C Unaffected	D Unaffected	E Affected	H Affected	I Unaffected	Segregated in seven family members
Exonic, splicing	10089	10064	10079	10065	10230	10194	10216	64
Nonsynonymous, splicing, indel, nonsense	4987	5020	5055	5038	5143	5234	5200	32
Allele frequency not available	577	600	536	555	671	794	786	2

chromosome 17 (at 5 cM, with a maximum LOD score of 2.53). In the second detailed linkage analysis, these peaks were determined to range from 167.49 cM at rs4233674 at position 159 058 679 to 168.19 cM at rs7598162 at position 160 935 582, and from 181.23 cM at rs4402725 at position 174 893 412 to 187.05 cM at rs7420169 at position 182 548 671 on chromosome 2; from 26.42 cM at rs2736043 at position 15 713 330 to 34.88 cM at rs9325871 at position 20 391 160, and from 61.02 cM at rs6999814 at position 41 660 854 to 62.32 cM at rs10957281 at position 49 769 454 on chromosome 8; and from 4.7 cM at rs11078552 at position 1 550 848 to 5.45 cM at rs1057355 at position 1 657 899 on chromosome 17. Haplotypes shared by affected individuals in these regions were confirmed by visual inspection. There were a few incompatible SNPs in these regions, presumably due to genotyping error.

Exome sequencing and segregation analysis
In exome sequencing, an average of 215 million reads enriched by SureSelect v4 (SSv4) and 319 million reads enriched by SureSelect v2 (SSv2) were generated, and 99% of reads were mapped to the

reference genome by Burrows-Wheeler Alignment tool. An average of 57% (SSv4) and 61% (SSv2) of those reads were duplicated and removed, and an average of 80% (SSv4) and 66% (SSv2) of mapped reads without duplicates were in target regions. The average coverage of each exome was 163-fold (SSv4) and 130-fold (SSv2). An average of 85% (SSv4) and 69% (SSv2) of target regions were covered at least 50-fold (Supplementary Table 2). On average, 10133 SNVs or indels, which are located within coding exons or splice sites, were identified per individual (Table 1). A total of 64 variants were common among patients and not present in unaffected individuals, and 32 of those were left after excluding synonymous SNVs. In these variants, only the heterozygous mutation c.90263G>T (NM_001256850) at position 179 410 777 of chromosome 2, which was predicted to p.W30088L in *TTN*, was novel (that is, not present in dbSNP v135 or 1000 genomes). Polyphen2 predicted this mutation as probably damaging. This mutation was located in a candidate region suggested by the linkage analysis in the present study. The other variants were registered with dbSNP135, and the allele frequencies, except for one SNV, rs138183879, in *IKBKB*, ranged from 0.0023 to 0.62.
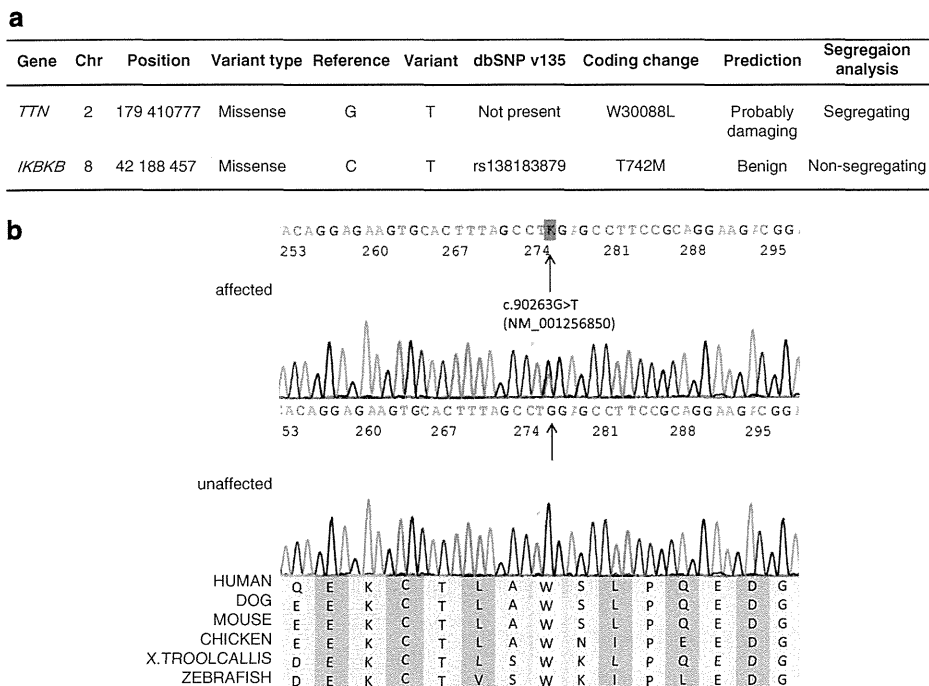
Figure 4 Identified mutations by exome sequencing. (a) We performed segregation analysis of two candidates. (b) The identified *TTN* mutation and its conservation among species. Sanger sequencing confirmed the heterozygous G to T substitution (indicated by the arrow) at the position chr2;179 410 777, which corresponds to c.90263G>T in exon 293 (NM_001256850.1). The substitution leads to p.W30088L (NP_001243779.1), and this amino acid is conserved among species.

These values were not compatible with the assumption that MFM was a rare disease and showed complete penetrance in this family. The allele frequency of rs138183879 was not available in dbSNP135, and this SNV was in the candidate region on chromosome 8 based on linkage analysis.

We then performed a segregation analysis on the two candidates, the novel mutation c.90263G>T in *TTN* and rs138183879 in *IKBKB*, through Sanger sequencing in 10 family members (A–J in Figure 1; Figure 4a). The rs138183879 SNP was not found in individual J, that is, it was not segregated with the disease in this family. In contrast, the novel mutation c.90263G>T in *TTN* was detected in all patients (n = 5) and not detected in any of the unaffected family members (n = 5) or 191 ethnically matched control subjects (382 chromosomes). These results suggested that this rare mutation in *TTN* segregated with the disease in this family.

DISCUSSION

In this study, we found that a novel missense mutation in *TTN* segregated with MFM in a large Japanese family. The identified c.90263G>T mutation in *TTN* (NM_001256850) was considered to be the genetic cause of MFM in our family, because (1) exome sequencing revealed that this was the best candidate mutation after filtering SNPs and indels, (2) this mutation is located in a region on chromosome 2 shared by affected family members, (3) the segregation with MFM was confirmed by Sanger sequencing, (4) this mutation was not detected in 191 control individuals, (5) this mutation was predicted to alter highly conserved amino acids (Figure 4b) and (6) *TTN* encodes a Z-disc-binding molecule called titin, which is similar to all of the previously identified causative genes for MFMs, which also encode Z-disc-associated molecules.

Recently, three mutations in *TTN* have been reported as the causes of hereditary myopathy with early respiratory failure (HMERF,

MIM #603689),[11–16] which has similar muscle pathology to MFMs. The identified novel missense mutation c.90263G>T in our study was located on the same exon as recently reported HMERF mutations: c.90272C>T in a Portuguese family[16] and c.90315T>C in Swedish and English families[14,15] (Table 2). This finding suggests the possibility that our family can be recognized as having HMERF from a clinical aspect.

Compared with symptoms described in the past three reports on HMERF (also see Table 2), our patients have common features, such as autosomal dominant inheritance, early respiratory failure, the absence of clinically apparent cardiomyopathy, normal to mild elevation of serum CK and histological findings compatible with MFM. Early involvement of the tibialis anterior is also common, except for the Portuguese family, who reported isolated respiratory insufficiency and a milder presentation of HMERF. Thus, our family shares major clinical manifestations with patients with HMERF, suggesting that the identified mutation is novel for MFM and HMERF.

To date, mutations in *TTN* have been identified in skeletal myopathy and cardiomyopathy.[17,18] The relationship between the variant positions on *TTN* and phenotypes accompanied by skeletal or respiratory muscle involvement is summarized in Table 2. Titin is a large protein (4.20 MDa) that extends from the Z-disk to the M-line within the sarcomere, and it is composed of four major domains: Z-disc, I-band, A-band and M-line (Figure 5). All four HMERF mutations detected by other groups and our study were consistently located in the A-band domain, while mutations in tibial muscular dystrophy (TMD) (MIM #600334),[19–24] limb-girdle muscular dystrophy type 2J (LGMD2J) (#608807)[19,25] and early-onset myopathy with fatal cardiomyopathy (#611705)[26] were located in the M-line domain. HMERF and TMD have some common clinical characteristics, such as autosomal dominant inheritance with onset in adulthood and strong involvement of the tibialis anterior muscle.

Table 2 Previously reported TTN mutations with skeletal and/or respiratory muscle involvement

Phenotype	LGMD	HMERF	Our family	HMERF	HMERF	TMD	TMD	LGMD2J	TMD	TMD	TMD	TMD	TMD	Early-onset myopathy with fatal cardiomyopathy	Early-onset myopathy with fatal cardiomyopathy
Reported by	Vasli et al.[16]	Ohlsson et al.,[14] Pfeffer et al.[15]	Abe et al.[5]	Vasli et al.[16]	Edstrom et al.,[12] Nicolao, et al.[11] Lang e et al.[13]	Hackman et al.[23]	Udd et al.,[20] Hackman et al.[19]	Udd et al.,[25] Hackman et al.[19]	Pollazzon et al.[24]	Van den Bergh et al.[22]	Seze et al.,[21] Hackman et al.[19]	Hackman et al.[23]	Hackman et al.[23]	Carmignac et al.[26]	Carmignac et al.[26]
Mutation identified in Nucleotide (NM_001256850.1)	2012 c.3100G>A, c.52024G>A	2012 c.90315T>C	2012 c.90263G>T	2012 c.90272C>T	2005 c.97348C>T	2008 c.102724delT	2002 102857_102867del11ins11	2002 102857_102867del11ins11	2010 c.102914A>C	2003 c.102917T>A	2002 c.102944T>C	2008 c.102966delA	2008 c.102967C>T	2007 g.289385delACCAAGTG	2007 g.291297delA
Protein (NP_001243779.1)	p.V1034M, p.A17342T	p.C30071R	p.W30088L	p.P30091L	p.R32450W				p.H34305P	p.I34306N	p.L34315P		p.Q34323X		
Domain	I-band, A-band	A-band (Fn3)	A-band (Fn3)	A-band (Fn3)	A-band (kinase)	M-line	M-line	M-line	M-line	M-line	M-line	M-line	M-line	M-line	M-line
Population Inheritance	French AR	Swedish English AD	Japanese AD	Portuguese AD	Swedish AD	French AD	Finnish AD	Finnish AR	Italian AD	Belgian AD	French AD	Spanish AD	French AD	Sudanese Consanguineous siblings	Moroccan Consanguineous siblings
Onset	35	33–71	27–45	46	20–50s	20–30s	35–55	20–30s	50–60s	47	45	40–50s	30s	Neonatal	Infant-early childhood
Skeletal muscles															
Major	Proximal UL and LL	TA, PL, EDL, ST	TA, ST	No	TA, neck flexor, proximals	TA, GA,HAM, pelvic	TA	All proximals	TA	TA	TA	TA	TA, HAM, pelvic	General muscle weakness and hypotonia	Psoas, TA, GA, peroneus
Minor		Neck flexor	Cervical, shoulder girdles, intercostals, proximal limb			QF				EDL, peroneal, TP	GA, femoral, scapular	HAM, GA	GA, distal UL		QF, proximal UL, neck, facial, trunk flexor
Spared			Facial			Proximal UL	Facial, UL, proximals	Facial		UL, proximal LL	Facial	UL	Proximal UL, QF		
Cardiac muscles	ND	No	No	ND	ND	ND	No	No	ND	ND	ND	ND	ND	DCM, onset; in the first decade	DCM, onset; 5–12 years old
Respiratory failure	ND	Yes, within 5–8 years	Yes, within 7 years	Isolated respiratory failure	Yes, as first presentation	ND	ND	ND	ND	ND	ND	ND	ND	ND	ND
Muscle pathologic features	ND	Inclusion bodies (major) and RVs (minor)	Cytoplasmic bodies (major) and RVs (minor)	Cytoplasmic bodies	Cytoplasmic bodies, positive for rhodamine-conjugated phalloidin	Dystrophic pattern without vacuoles	Nonspecific dystrophic change	Nonspecific dystrophic change, loss of calpain-3.	Dystrophic pattern with RVs	Nonspecific, RV	Nonspecific	Dystrophic pattern with RVs	Nonspecific	Minicore-like lesions and abundant central nuclei	Minicore-like lesions and abundant central nuclei

Abbreviations: AD, autosomal dominant; AR, autosomal recessive; DCM, dilated cardiomyopathy; EDL, extensor digitorum longus; GA, gastrocnemius; HAM, hamstrings; LL, lower limb; ND, not described; no, no involvement; PL, peroneus longus; QF, quadriceps femoris; RV, rimmed vacuole; ST, semitendinosus; TA, tibialis anterior; TMD, tibial muscular dystrophy; TP, tibialis posterior; UL, upper limb.
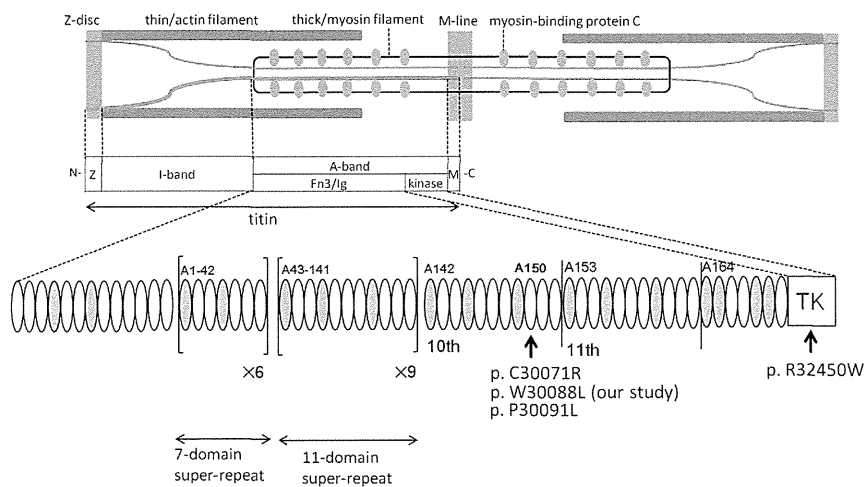
Figure 5 Structure of titin and mutation distribution in the A-band domain. Human *TTN* was mapped to 2q31.2. *TTN* is 294 kb and is composed of 363 exons that code for a maximum of 38 138 amino-acid residues and a 4.20-MDa protein[32] called titin. Titin is expressed in the cardiac and skeletal muscles and spans half the sarcomere, with its N-terminal at the Z-disc and the C-terminal at the M-line.[33] Titin is composed of four major domains: Z-disc, I-band, A-band and M-line. I-band regions of titin are thought to make elastic connections between the thick filament (that is, myosin filament) and the Z-disc within the sarcomere, whereas the A-band domain of titin seems to be bound to the thick filament, where it may regulate filament length and assembly.[34] The gray and white ellipses indicate an Ig-like domain and fibronectin type 3 domain, respectively. Our mutation (p.W30088L) and the neighboring two mutations (that is, p.C30071R and p.P30091L) were all located in the 6th Fn3 domain in the 10th domain of large super-repeats. A full color version of this figure is available at the *Journal of Human Genetics* journal online.

In contrast, one of the distinctive features of TMD is that early respiratory failure has not been observed in patients with TMD. Histological findings of TMD usually do not include CBs but show nonspecific dystrophic change. The underlying pathogenic processes explaining why mutations on these neighboring domains share some similarities but also some differences are unknown.

Three of four HMERF mutations in the A-band domain are located in the fibronectin type 3 and Ig-like (Fn3/Ig) domain, and one of four HMERF mutations is located in the kinase domain (Table 2, also see Figure 5). The missense mutation c.97348C > T in the kinase domain was the first reported HMERF mutation. It has been shown that the kinase domain has an important role in controlling muscle gene expression and protein turnover via the neighbor of BRCA1 gene-1-muscle-specific RING finger protein-serum response transcription factor pathway.[13] Moreover, the Fn3/Ig domain is composed of two types of super-repeats: six consecutive copies of 7-domain super-repeat at the N-terminus and 11 consecutive copies of 11-domain super-repeat at the C-terminus.[27-29] These super-repeats are highly conserved among species and muscles. Our identified mutation (c.90263G > T) and the neighboring two mutations (that is, c.90272C > T and c.90315T > C shown in Table 2) were all located on the 6th Fn3 domain in the 10th copy of 11-domain super-repeat (that is, A150 domain[30]) (Figure 5). Although some Fn3 domains are proposed to be the putative binding site for myosin,[31] the role with the majority of Fn3 domains, how it supports the structure of each repeat architecture, and the identity of its binding partner have not been fully elucidated. Our findings suggested that the Fn3 domain, in which mutations clustered, has critical roles in the pathogenesis of HMERF, although detailed mechanisms of pathogenesis remain unknown.

In conclusion, we have identified a novel disease-causing mutation in *TTN* in a family with MFM that was clinically compatible with HMERF. Because of its large size, global mutation screening of *TTN* has been difficult. Mutations in *TTN* may be detected by massively parallel sequencing in more patients with MFMs, especially in patients with early respiratory failure. Further studies are needed to understand the genotype–phenotype correlations in patients with mutations in *TTN* and the molecular function of titin.

1 Nakano, S., Engel, A. G., Waclawik, A. J., Emslie-Smith, A. M. & Busis, N. A. Myofibrillar myopathy with abnormal foci of desmin positivity. I. Light and electron microscopy analysis of 10 cases. *J. Neuropathol. Exp. Neurol.* **55,** 549–562 (1996).
2 Olive, M., Odgerel, Z., Martinez, A., Poza, J. J., Bragado, F. G., Zabalza, R. J. et al. Clinical and myopathological evaluation of early- and late-onset subtypes of myofibrillar myopathy. *Neuromuscul. Disord.* **21,** 533–542 (2011).
3 Olive, M., Goldfarb, L. G., Shatunov, A., Fischer, D. & Ferrer, I. Myotilinopathy: refining the clinical and myopathological phenotype. *Brain* **128,** 2315–2326 (2005).
4 Selcen, D. & Engel, A. G. Myofibrillar myopathy caused by novel dominant negative alpha B-crystallin mutations. *Ann. Neurol.* **54,** 804–810 (2003).
5 Abe, K., Kobayashi, K., Chida, K., Kimura, N. & Kogure, K. Dominantly inherited cytoplasmic body myopathy in a Japanese kindred. *Tohoku. J. Exp. Med.* **170,** 261–272 (1993).
6 Abecasis, G. R., Cherny, S. S., Cookson, W. O. & Cardon, L. R. Merlin–rapid analysis of dense genetic maps using sparse gene flow trees. *Nat. Genet.* **30,** 97–101 (2002).
7 Li, H. & Durbin, R. Fast and accurate short read alignment with Burrows-Wheeler transform. *Bioinformatics* **25,** 1754–1760 (2009).
8 McKenna, A., Hanna, M., Banks, E., Sivachenko, A., Cibulskis, K., Kernytsky, A. et al. The Genome Analysis Toolkit: a MapReduce framework for analyzing next-generation DNA sequencing data. *Genome. Res.* **20,** 1297–1303 (2010).
9 Wang, K., Li, M. & Hakonarson, H. ANNOVAR: functional annotation of genetic variants from high-throughput sequencing data.. *Nucleic Acids Res.* **38,** e164 (2010).
10 Adzhubei, I. A., Schmidt, S., Peshkin, L., Ramensky, V. E., Gerasimova, A., Bork, P. et al. A method and server for predicting damaging missense mutations. *Nat. Methods* **7,** 248–249 (2010).
11 Nicolao, P., Xiang, F., Gunnarsson, L. G., Giometto, B., Edstrom, L., Anvret, M. et al. Autosomal dominant myopathy with proximal weakness and early respiratory muscle involvement maps to chromosome 2q. *Am. J. Hum. Genet.* **64,** 788–792 (1999).

12 Edstrom, L., Thornell, L. E., Albo, J., Landin, S. & Samuelsson, M. Myopathy with respiratory failure and typical myofibrillar lesions. *J. Neurol. Sci.* **96**, 211–228 (1990).

13 Lange, S., Xiang, F., Yakovenko, A., Vihola, A., Hackman, P., Rostkova, E. *et al.* The kinase domain of titin controls muscle gene expression and protein turnover. *Science* **308**, 1599–1603 (2005).

14 Ohlsson, M., Hedberg, C., Bradvik, B., Lindberg, C., Tajsharghi, H., Danielsson, O. *et al.* Hereditary myopathy with early respiratory failure associated with a mutation in A-band titin. *Brain* **135**, 1682–1694 (2012).

15 Pfeffer, G., Elliott, H. R., Griffin, H., Barresi, R., Miller, J., Marsh, J. *et al.* Titin mutation segregates with hereditary myopathy with early respiratory failure. *Brain* **135**, 1695–1713 (2012).

16 Vasli, N., Bohm, J., Le Gras, S., Muller, J., Pizot, C., Jost, B. *et al.* Next generation sequencing for molecular diagnosis of neuromuscular diseases. *Acta. Neuropathol.* **124**, 273–283 (2012).

17 Kontrogianni-Konstantopoulos, A., Ackermann, M. A., Bowman, A. L., Yap, S. V. & Bloch, R. J. Muscle giants: molecular scaffolds in sarcomerogenesis. *Physiol. Rev.* **89**, 1217–1267 (2009).

18 Ottenheijm, C. A. & Granzier, H. Role of titin in skeletal muscle function and disease. *Adv. Exp. Med. Biol.* **682**, 105–122 (2010).

19 Hackman, P., Vihola, A., Haravuori, H., Marchand, S., Sarparanta, J., De Seze, J. *et al.* Tibial muscular dystrophy is a titinopathy caused by mutations in TTN, the gene encoding the giant skeletal-muscle protein titin. *Am. J. Hum. Genet.* **71**, 492–500 (2002).

20 Udd, B., Partanen, J., Halonen, P., Falck, B., Hakamies, L., Heikkila, H. *et al.* Tibial muscular dystrophy. Late adult-onset distal myopathy in 66 Finnish patients. *Arch. Neurol.* **50**, 604–608 (1993).

21 de Seze, J., Udd, B., Haravuori, H., Sablonniere, B., Maurage, C. A., Hurtevent, J. F. *et al.* The first European family with tibial muscular dystrophy outside the Finnish population. *Neurology* **51**, 1746–1748 (1998).

22 Van den Bergh, P. Y., Bouquiaux, O., Verellen, C., Marchand, S., Richard, I., Hackman, P. *et al.* Tibial muscular dystrophy in a Belgian family. *Ann. Neurol.* **54**, 248–251 (2003).

23 Hackman, P., Marchand, S., Sarparanta, J., Vihola, A., Penisson-Besnier, I., Eymard, B. *et al.* Truncating mutations in C-terminal titin may cause more severe tibial muscular dystrophy (TMD). *Neuromuscul. Disord.* **18**, 922–928 (2008).

24 Pollazzon, M., Suominen, T., Penttila, S., Malandrini, A., Carluccio, M. A., Mondelli, M. *et al.* The first Italian family with tibial muscular dystrophy caused by a novel titin mutation. *J. Neurol.* **257**, 575–579 (2010).

25 Udd, B., Rapola, J., Nokelainen, P., Arikawa, E. & Somer, H. Nonvacuolar myopathy in a large family with both late adult onset distal myopathy and severe proximal muscular dystrophy. *J. Neurol. Sci.* **113**, 214–221 (1992).

26 Carmignac, V., Salih, M. A., Quijano-Roy, S., Marchand, S., Al Rayess, M. M., Mukhtar, M. M. *et al.* C-terminal titin deletions cause a novel early-onset myopathy with fatal cardiomyopathy. *Ann. Neurol.* **61**, 340–351 (2007).

27 Labeit, S., Barlow, D. P., Gautel, M., Gibson, T., Holt, J., Hsieh, C. L. *et al.* A regular pattern of two types of 100-residue motif in the sequence of titin. *Nature* **345**, 273–276 (1990).

28 Labeit, S. & Kolmerer, B. Titins: giant proteins in charge of muscle ultrastructure and elasticity. *Science* **270**, 293–296 (1995).

29 Tskhovrebova, L., Walker, M. L., Grossmann, J. G., Khan, G. N., Baron, A. & Trinick, J. Shape and flexibility in the titin 11-domain super-repeat. *J. Mol. Biol.* **397**, 1092–1105 (2010).

30 Bucher, R. M., Svergun, D. I., Muhle-Goll, C. & Mayans, O. The structure of the FnIII Tandem A77-A78 points to a periodically conserved architecture in the myosin-binding region of titin. *J. Mol. Biol.* **401**, 843–853 (2010).

31 Muhle-Goll, C., Habeck, M., Cazorla, O., Nilges, M., Labeit, S. & Granzier, H. Structural and functional studies of titin's fn3 modules reveal conserved surface patterns and binding to myosin S1–a possible role in the Frank-Starling mechanism of the heart. *J. Mol. Biol.* **313**, 431–447 (2001).

32 Bang, M. L., Centner, T., Fornoff, F., Geach, A. J., Gotthardt, M., McNabb, M. *et al.* The complete gene sequence of titin, expression of an unusual approximately 700-kDa titin isoform, and its interaction with obscurin identify a novel Z-line to I-band linking system. *Circ. Res.* **89**, 1065–1072 (2001).

33 Maruyama, K., Yoshioka, T., Higuchi, H., Ohashi, K., Kimura, S. & Natori, R. Connectin filaments link thick filaments and Z lines in frog skeletal muscle as revealed by immunoelectron microscopy. *J. Cell. Biol.* **101**, 2167–2172 (1985).

34 Guo, W., Bharmal, S. J., Esbona, K. & Greaser, M. L. Titin diversity–alternative splicing gone wild. *J. Biomed. Biotechnol.* **2010**, 753675 (2010).

Supplementary Information accompanies the paper on Journal of Human Genetics website (http://www.nature.com/jhg)

Clinical Medicine Insights: Case Reports

CASE REPORT

Balloon Dilation in Sporadic Inclusion Body Myositis Patients with Dysphagia

Ken-ya Murata[1], Ken Kouda[2], Fumihiro Tajima[2] and Tomoyoshi Kondo[1]

[1]Department of Neurology, [2]Department of Rehabilitation Medicine, Wakayama Medical University, Wakayama, Japan. Corresponding author email: kemurata@wakayama-med.ac.jp

Abstract: Here, we describe balloon catheter dilation at the upper esophageal sphincter (UES) in three sporadic inclusion body myositis (s-IBM) patients with dysphagia. Initially, we performed IVIg therapy, and, three months later, switched to balloon dilation therapy. A 12-Fr balloon catheter was inserted from the mouth under fluoroscopy and the balloon inflated at the UES. The catheter was pulled back and re-inserted several times. We examined videofluoroscopy (VF) and pressure at the oropharynx, hypopharynx and UES using computed pharyngoesophageal manometry (CPM). Before both therapies, the VF study revealed a very small amount of barium paste passing through the UES. After balloon dilation therapy, as well as IVIg, subjective complaints of dysphagia disappeared and the VF study revealed an increased amount of barium paste passing through the UES. We conclude that balloon dilation therapy is a complementary method for conventional dysphagia therapies in s-IBM patients with dysphagia.

Keywords: balloon dilation, computed pharyngoesophageal manometry, cricopharyngeal achalasia, dysphagia, sporadic inclusion body myositis

Introduction

Sporadic inclusion body myositis (s-IBM) is an inflammatory myopathy characterized by selectivity of muscle involvement, finger flexor and/or quadriceps femoris involvement, and a chronic progressive corticosteroid-resistant course.[1] Dysphagia has been reported in approximately one-third of s-IBM patients,[2] and patients with progressive dysphagia have a significantly poorer functional rating than patients with non-progressive dysphagia.

In the current study, we performed dilation of the upper esophageal sphincter (UES) using a balloon catheter (balloon dilation) in s-IBM patients with dysphagia. We compared the efficacy of this therapy with intravenous immunoglobulin (IVIg) therapy using videofluoroscopy (VF) and computed pharyngoesophageal manometry (CPM).

Materials and Methods

This study was performed using 3 s-IBM patients with dysphagia (2 males and 1 female; average age, 78.3 ± 4.5 years; average disease duration, 10.0 ± 5.3 years) at the Department of Neurology in Wakayama University between January 2008 and December 2010 (Table 1). These patients fulfilled the proposed diagnostic criteria for s-IBM.[3] The study was approved by the ethics committee of the Faculty of Medicine at Wakayama Medical University. All patients provided written informed consent in order to be included in the study.

First, we performed IVIg therapy (400 mg/kg/day for 5 days) on the three patients. Three months after IVIg treatment, we performed balloon dilation therapy. A 12-Fr balloon catheter for bladder placement was inserted from the mouth to the region of the UES including the cricopharyngeal muscle. The insertion position of the catheter was confirmed using fluoroscopy. The UES was then dilated by balloon inflation to 18 mm and then 20 mm (Fig. 1B). The catheter

was pulled back, re-inserted and dilated several times during dry swallowing. Once the insersion position was determined, the patients themselves were able to insert the catheter at the best position without fluroscopy. This procedure was straightforward, and patients performed balloon therapy alone at home.

Swallowing was assessed before and after the two therapies using videofluoroscopy (VF)[4] and computed pharyngoesophageal manometry (CPM).[5] For VF, patients were placed upright and the oropharynx was viewed in lateral and anterior-posterior projections. Three mL of liquid barium and paste barium were administered by teaspoon. Swallowing examinations were repeated in different upright positions. For CPM, a sequential computer manometry system (PC polygraph; Medtronic, Medtronic Parkway, Minneapolis) with a 4-intraluminal pressure transducer assembly (Mui Scientific, Mississauga, Ontario) was used with the recording sites set 5 cm apart. The assembly was placed transnasally and recording sites were selected at the oropharynx, hypopharynx, UES, and proximal esophagus (Fig. 2A). We evaluated UES pressure, along with pharyngeal and esophageal peristalsis, during barium swallowing. We also performed VF and CPM studies on ten aged-matched healthy volunteers without neuromuscular disease as controls.

Results
Clinical symptoms

Prior to both therapies, it was difficult for the three subjects to eat even half-solid meals. Following IVIg therapy, status improved and the three patients were able to eat regular meals. Effectiveness endured for two months following single dose therapy. We were able to successfully perform balloon dilation in only 2 (patients 2 and 3) out of the 3 subjects, because a severe pharyngeal reflex in patient 1 prevented insertion of the catheter into the pharyx. In the two patients receiving balloon dilation, dysphagia improved and

Table 1. s-IBM patient profiles.

Patient	Sex	Complaint of dysphagia	Age	Duration of disease (years)	Aid for walking	CK (IU/L)	Complications
1	M	(+)	83	4	Cane	186	Hepatitis C
2	F	(+)	79	12	Walker	482	HT, LS
3	M	(+)	74	14	Cane	691	HT

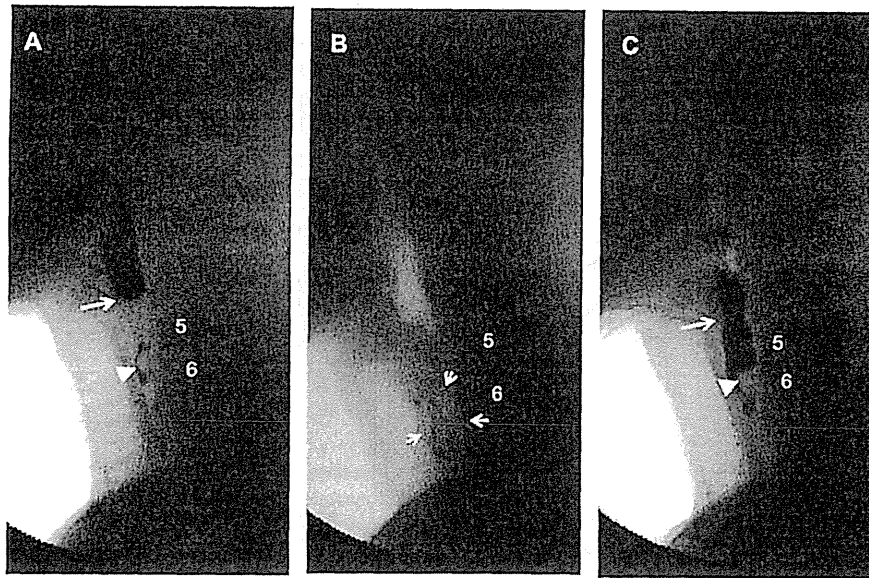Abbreviations: HT, Hypertension; LS, Lumbar spondylosis.

Figure 1. Videofluoroscopy in an s-IBM patient (Patient 2) using barium paste (A and C) and during balloon dilation therapy (B).
Notes: The barium paste is concentrated at the UES opening sites before balloon therapy (A, arrow) and is passed through the UES after balloon therapy (C, arrow). The expanded balloon (B, surrounded by arrows) pushes against the crycopharyngeal muscles. Pharyngeal muscle propulsions (PP; arrow head) were observed in the UES at the position of the crycopharyngeal muscle (A and C). The sites and shapes of PP remained unchanged before (A) and after (C) balloon therapy.

it became possible to eat regular meals. During the first two weeks, patients performed balloon dilation therapy once a day to eat regular meals. However, the effect of balloon therapy weakened and it became necessary to perform this therapy several times before each meal every day. Once balloon dilation therapy was performed, patients were easily able to eat meals for 30 minutes on each occasion. These two patients could eat regular meals for at least one year by simply performing balloon dilation therapy. No adverse effects were recorded in relation to performing balloon dilation.

Videofluoroscopy (VF)

Prior to IVIg and balloon dilation therapies, VF results indicated that all patients exhibited a normal oral phase of swallowing but possessed abnormalities in the pharyngeal phase. The UES opening was impaired and aspiration was confirmed due to an influx of remaining food from the piriform recess (Fig. 1A).

After IVIg therapy, the amount of barium paste passing through the entrance of the UES increased (data not shown). Following both balloon and IVIg therapy, the amount of barium passing through the entrance of the UES increased (Fig. 1C). We could

confirm these effects at least one year later, following introduction of of of the first balloon dilation thearpy. As a consequence, food residues in the piriform recess were reduced, and aspiration of food residues was alleviated by both therapies.

In all cases, the cricopharyngeal prominence (CP) was confirmed at the UES including the cricopharyngeal muscle (C5–6; Fig. 1A and C arrow head). CP was also observed at the inferior pharyngeal constrictor muscle (C2–3) in patient 3 (data not shown). The size and site of the CP did not differ when compared before and after IVIg and balloon therapies (Fig. 1A and C arrow head).

Computed pharyngoesophageal manometry (CPM)

In normal healthy control subjects, the pharyngeal peak pressure at the oropharynx and hypopharynx was elevated simultaneously (Fig. 2B, 1 and 2). Contrary to the high pharyngeal pressure at the oropharynx and hypopharynx, the pressure at the UES decreased until the UES opened (nadir deglutitive UES pressure; Fig. 2B-3, arrow). After the barium paste passed through the entrance of the UES, pharyngeal pressure at the UES increased (Fig. 2B-3, asterisk).
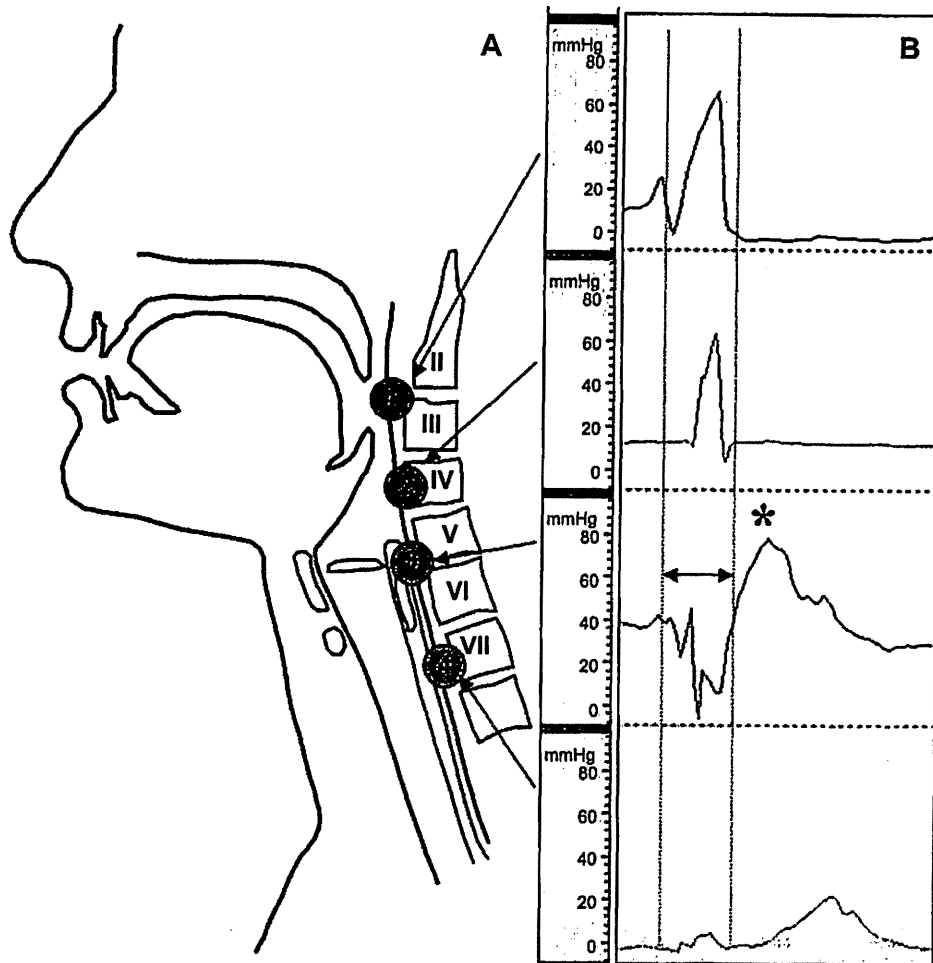
Figure 2. Manometry study of normal control. (A) Manometry study using simultaneous 4-channel pressure recording during 3 ml barium swallowing. channel 1 = oropharynx; channel 2 = hypopharynx; channel 3= UES; channel 4 = proximal esophagus. (B) Manometric findings in a healthy control subject. Notes: The pharyngeal peak pressure at the oropharynx and hypopharynx elevated simultaneously (1 and 2). Contrary to the high pharyngeal pressure at the oropharynx and hypopharynx, the pressure at the UES decreased until the UES opened (nadir deglutitive UES pressure; 3, arrow). After the barium paste passed through the entrance of the UES, pharyngeal pressure at the UES increased (3, asterisk).

Before IVIg and balloon dilation, the peak pressure of the oropharynx, hypopharynx and UES in s-IBM patients was very low compared with that of normal controls (Fig. 3A-1–3 and 3C-1–3). Nadir deglutitive UES pressure was not observed in s-IBM patients (Fig. 3A-3 and 3C-3). Following IVIg therapy, although nadir deglutitive UES pressure was not observed (Fig. 3B-3), the peak pressure of the hypopharynx and UES became elevated (Fig. 3B-2 and 3).

After balloon dilation, although nadir deglutitive UES pressure was not observed (Fig. 3C-3), the peak pressure of the oropharynx and hypopharynx was elevated (Fig. 3D-1 and 2). The contraction muscle power of the UES increased to the same level as that of normal controls (Fig. 3D-3, asterisk). Thirty minutes later,

internal pressure of the deglutition was re-determined and found to be the same as that immediately following balloon dilation. Consequently, we concluded that sustainability duration of the balloon dilation procedure was at least 30 minutes.

Discussion

Cricopharyngeal achalasia is defined as when the opening of the UES is not adequate during the pharyngeal phase, and a food mass is hard to pass.[6] Incomplete UES opening during swallowing has a number of different causes. Causes include impaired relaxation or spasm of the UES, such as hyperplasia and hypertrophy. They can also include fibrosis of the cricopharyngeal muscle, weakness of the suprahyoid
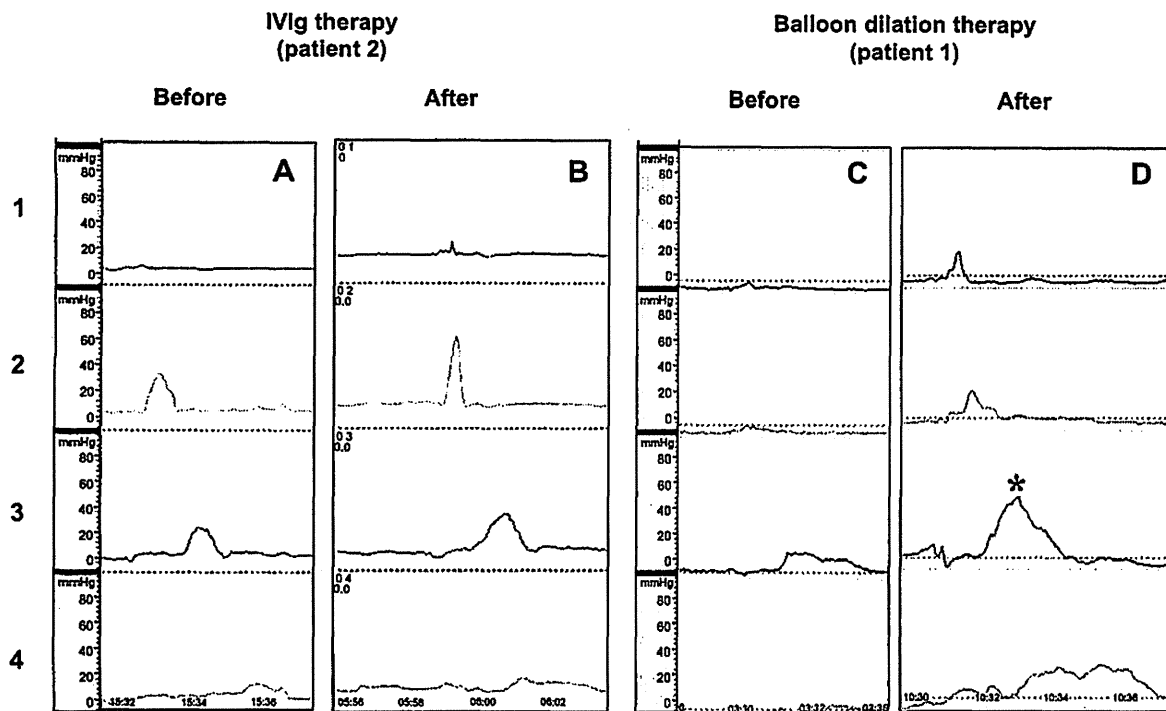
Figure 3. Manometry study of s-IBM patients. (A) Manometry during swallowing solid barium paste before IVIg therapy (patient 2). (B) Manometry during swallowing solid barium paste after IVIg therapy (patient 2). (C) Manometry during swallowing solid barium paste before balloon dilation therapy (patient 1) (D) Manometry during swallowing solid barium paste after balloon dilation therapy (patient 1) 1 = oropharynx; 2 = hypopharynx; 3 = UES; 4 = proximal esophagus.

Notes: Although the peak pressure at the oropharynx (A-1), hypopharynx (A-2) and UES (A-3) in patient 2 was low before therapy, the hypopharynx (B-2) and UES (B-3) pressures elevated after IVIg therapy. Nadir deglutitive UES pressure, which was observed in normal controls, was not observed both before (A-3) and after (B-3) therapy. The peak pressure at the oropharynx (C-1), hypopharynx (C-2) and UES (C-3) is almost 0 before balloon therapy, and is elevated remarkably after therapy (D-1-3). In particular, the peak pressure at the UES is similar to that of normal controls (D-3, asterisk). Nadir deglutitive UES pressure was not observed both before (C-3) and after (D-3) balloon therapy.

muscles, and diminished distending forces imparted by the bolus.[7] Because cricopharyngeal achalasia is considered a main reason for dysphagia in s-IBM patients, cricopharyngeal myotomy and botulinum toxin (BTX) therapy have been employed for dysphagia in s-IBM patients.[8] On the other hand, IVIg therapy has also been shown to be effective for s-IBM patients with dysphagia, although this treatment does not lead to significant improvement for limb muscle weaknesses.[9,10] Prior to IVIg therapy, our s-IBM patients suffered dysphagia. In addition, peak pressure of the oropharynx, hypopharynx and UES was low. Following IVIg therapies, the subjective complaint of dysphagia disappeared, and both the peak pressure of hypopharyngeal muscles and the contraction muscle power of the UES increased. Therefore, IVIg therapy improved the contraction power of pharyngeal and UES muscles.

Balloon dilation has been performed in patients with cricopharyngeal achalasia due to Wallenberg syndrome,[11] and in newborns with primary cricopharyngeal achalasia.[12,13] Prior to balloon dilation, it was difficult for the three s-IBM patients to eat even half-solid meals. The UES opening was impaired and aspiration due to an influx of food residue in the piriform recess was confirmed. After balloon therapy, the subjects were sucessfully able to eat regular meals, and the passage of a food mass through the UES was facilitated. In addition, the amount of barium paste passing through the UES increased, the amount of food residue in the piriform recess decreased, and aspiration with an influx of barium paste into the larynx disappeared.

An examination of cricopharyngeal muscle biopsies from s-IBM patients with severe dysphagia previously showed a marked increase in the replacement of endomysial connective tissue by fat, along with numerous small and round atrophic muscle fibers.[14] In the present study, UES contraction power was recovered by dilation of the crycopharyngeal muscles. These findings suggest that the number of UES muscle fibers